Supporting Information

Spatiotemporal Targeting of a Dual-Ligand Nanoparticle to Cancer Metastasis

Elizabeth Doolittle[1,2,3,†], Pubudu M. Peiris[1,2,3,†], Gilad Doron[1,3], Amy Goldberg[1,3], Samantha Tucci[1,3], Swetha Rao[1,3], Shruti Shah[1,3], Meilyn Sylvestre[1,3], Priya Govender[1,3], Oguz Turan[1,3], Zhenghong Lee[2,3,4], William P. Schiemann[4], and Efstathios Karathanasis[1,2,3,4*]

[1] Department of Biomedical Engineering, Case Western Reserve University, Cleveland, Ohio

[2] Department of Radiology, Case Western Reserve University, Cleveland, Ohio

[3] Case Center for Imaging Research, Case Western Reserve University, Cleveland, Ohio

[4] Case Comprehensive Cancer Center, Case Western Reserve University, Cleveland, Ohio

[†] These authors contributed equally to this work

[*] Author to whom correspondence should be addressed: Efstathios Karathanasis
email: stathis@case.edu

Contents

Nanoparticle (ID)	**Label** (type) *per particle*	**DPPC** *per particle*	**DSPE-PEG-peptide** *per particle*	**mPEG-DSPE** *per particle*
non-targeted (NT-NP)	2.76×10^3 (DSPE-Vivotag)	7.53×10^4	0	3.46×10^3
single-ligand (PSN-NP)	2.76×10^3 (DSPE-Vivotag)	7.53×10^4	2.57×10^3	0
single-ligand (RGD-NP)	2.76×10^3 (DSPE-Vivotag)	7.53×10^4	2.6×10^3	0
dual-ligand (dual-ligand-NP)	2.76×10^3 (DSPE-Vivotag)	7.19×10^4	5.35×10^3	0
dual-ligand (^{99m}Tc-dual-ligand-NP)	240 (DSPE-DTPA)	7.60×10^4	5.35×10^3	0

Supporting Table S1. Summary of the characteristics of each nanoparticle variant (amounts indicate molecules per nanoparticle).

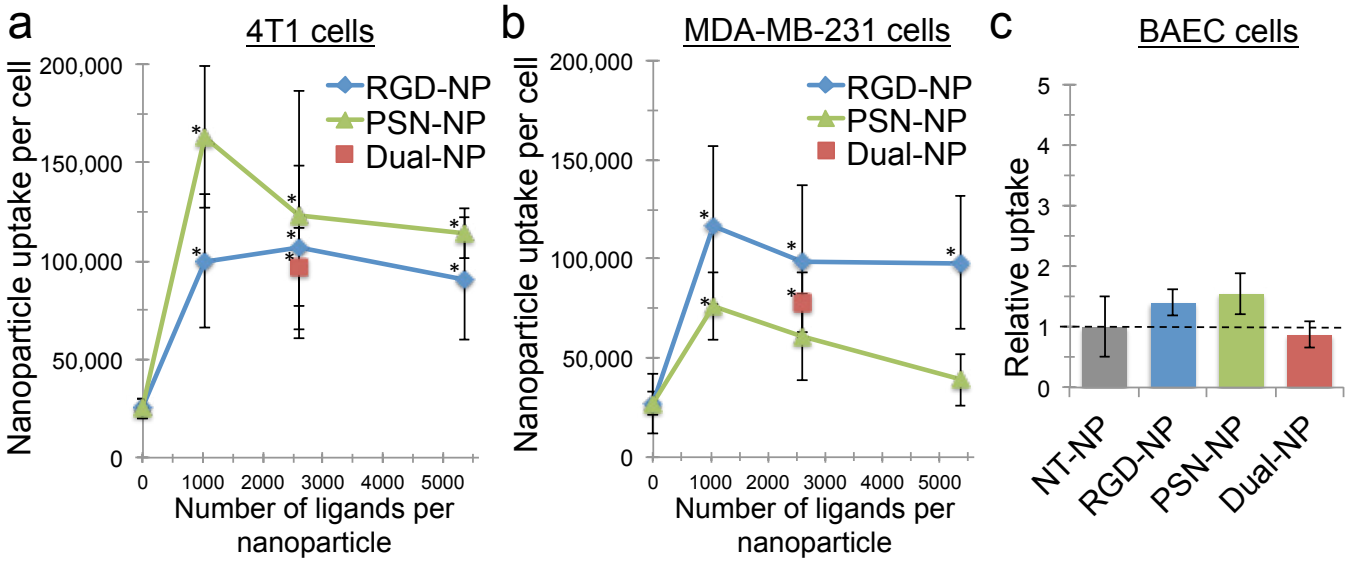

Supporting Figure S1. Cellular uptake in three cell types as a function of targeting ligands per nanoparticle. The targeting efficiency as a function of the number and type of ligand of the nanoparticle was evaluated in the two cell lines that were used in the animal studies (MDA-MB-231 and 4T1 cells) and bovine aortic endothelial cells (BAEC). The nanoparticle formulations (NT-NP, RGD-NP, PSN-NP and dual-ligand-NP) were labeled by loading a fluorophore into the nanoparticle that did not interfere with the targeting ligand on the distal end of the PEG. The cells were seeded in 24-well plates at a density of 50,000 cells per well. Prior to incubation with the nanoparticles, the cells were washed three times with fresh medium. Cells were then incubated for 3 h with an excess of nanoparticles at 37 °C in a 5% CO_2, high humidity environment. Following incubation, cells were placed on ice, washed three times and the fluorescence intensity was measured and analyzed (n=5 per condition; error bars denote standard deviation). The cellular uptake is shown as the number of nanoparticles per cell in the case of **(a)** 4T1 and **(b)** MDA-MB-231 cells. **(c)** The uptake by BAEC cells is normalized with respect to the NT-NP nanoparticles, which has relative uptake of 1 (* indicates statistical significance of the targeting nanoparticles to the values of the non-targeted variant (NT-NP); $P<0.05$; Student's t-test; n=5 per condition).

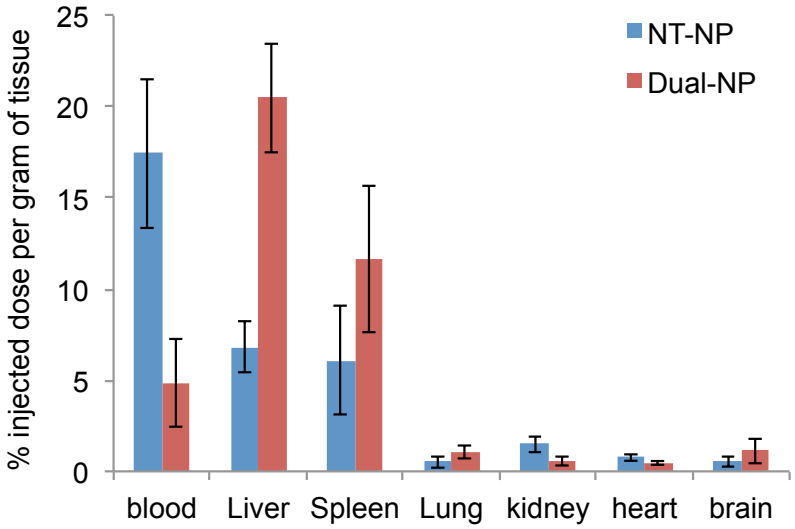

Supporting Figure S2. Organ distribution of dual-ligand and non-targeted nanoparticles in mice. Twenty four hours after intravenous injection of the dual-ligand (dual-NP) or non-targeted nanoparticles (NT-NP) at a dose of 3.7×10^{12} nanoparticles in each animal, the animals were anesthesized and transcardially perfused with heparinized PBS followed by 4% paraformaldehyde in PBS. As a component of the nanoparticle's liposomal bilayer, we used an Alexa 488-labeled phospholipid. In addition to blood collection, the organs were then retrieved, washed with PBS, blotted dry, and weighed. Tissue samples were prepared following an established protocol.[1] Briefly, the organs were homogenized in distilled, deionized water (20% wt/vol). Homogenates (200 µL) were mixed with 100 µL of 10% Triton X-100, 200 µL of water and 1500 µL of acidified isopropanol (0.75N HCl). Mixtures were stored overnight at -20 °C and then warmed at room temperature and vortexed for 5 min. After the samples were centrifuged at 5000g for 20 min, fluorescent readings of the suparnatants were obtained. For the blood samples, plasma was isolated by centrifugation (2200g, 15 min) followed by extraction using lysis in 30% MeOH and heating at 60 °C for 20 min. Organ samples from an animal treated with a saline injection were used to correct for background (n= 5 mice in each condition).

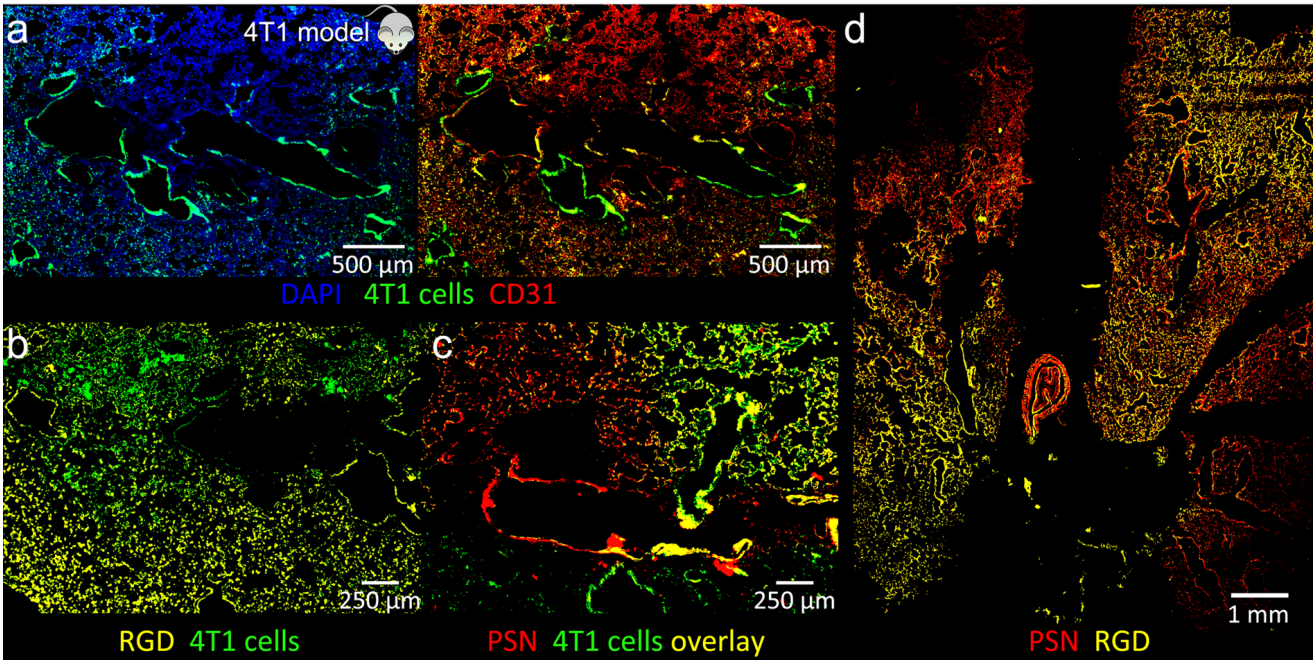

Supporting Figure S3. Histological evaluation of 4T1 metastases in the lungs of mice. (a) Fluorescence image of a histological section of a lung lobe (left panel: blue, nuclear stain (DAPI); green,

4T1 cancer cells). Images of entire sections of the organs were obtained using the automated tiling function of the microscope (10x magnification). In the same histological section, the location of metastatic cancer cells is shown with respect to endothelial cells (right panel: green, 4T1 cancer cells; red, endothelial cells). **(b)** Location of metastatic cancer cells is shown with respect to expression of $\alpha_v\beta_3$ integrin (green, 4T1 cancer cells; yellow, $\alpha_v\beta_3$ integrin). **(c)** Location of metastatic cancer cells is shown with respect to expression of P-selectin (green, 4T1 cancer cells; red, P-selectin). **(d)** In a large histological section, the expression of both $\alpha_v\beta_3$ integrin and P-selectin are shown (red, P-selectin; yellow, $\alpha_v\beta_3$ integrin).

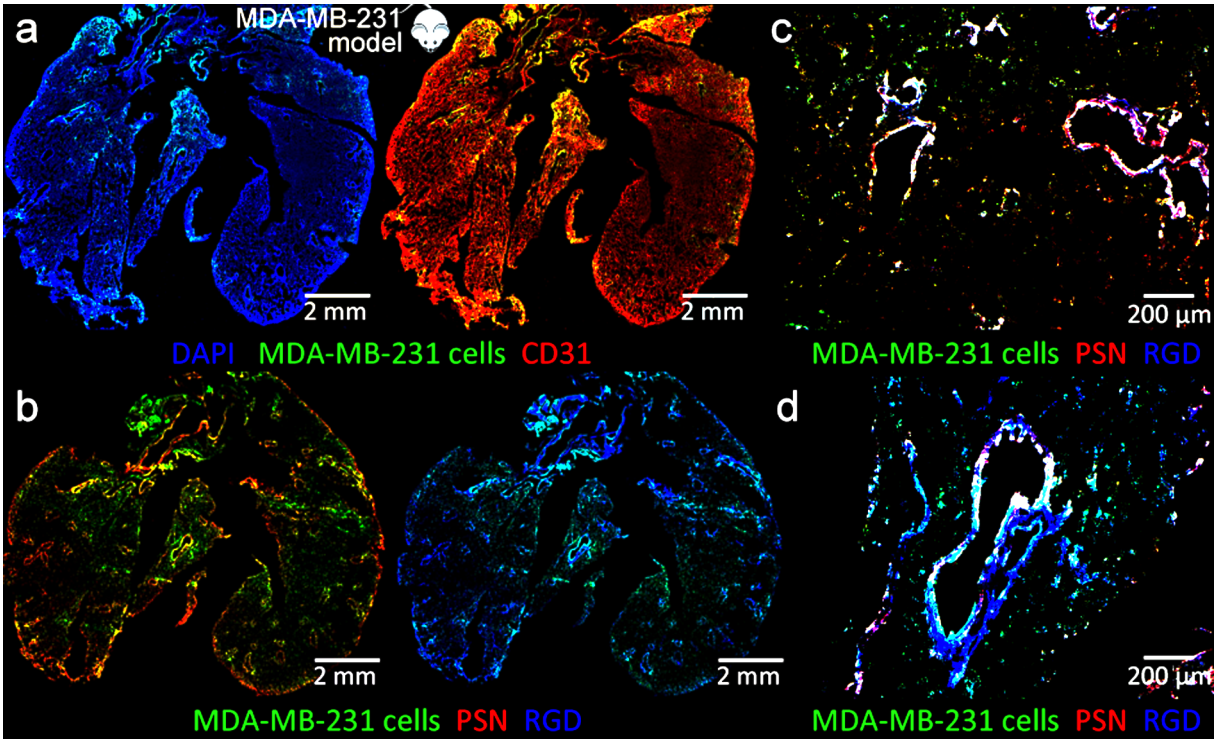

Supporting Figure S4. Histological evaluation of MDA-MB-231 metastases in the lungs of mice. (a) Fluorescence image of a large histological section of a lung (left panel: blue, nuclear stain (DAPI); green, MDA-MB-231 cancer cells). Images of entire histological sections of the organs were obtained using the automated tiling function of the microscope (10x magnification). In the same histological section, the location of metastatic cancer cells is shown with respect to endothelial cells (right panel: green, MDA-MB-231 cancer cells; red, endothelial cells). **(b)** In the same large histological section, the location of metastatic cancer cells is shown with respect to expression of P-selectin (left panel) and $\alpha_v\beta_3$ integrin (right panel). **(c-d)** In high magnification, the colocalization of metastatic cancer cells with the expression of both $\alpha_v\beta_3$ integrin and P-selectin is shown (green, 4T1 cancer cells; red, P-selectin; blue, $\alpha_v\beta_3$ integrin).

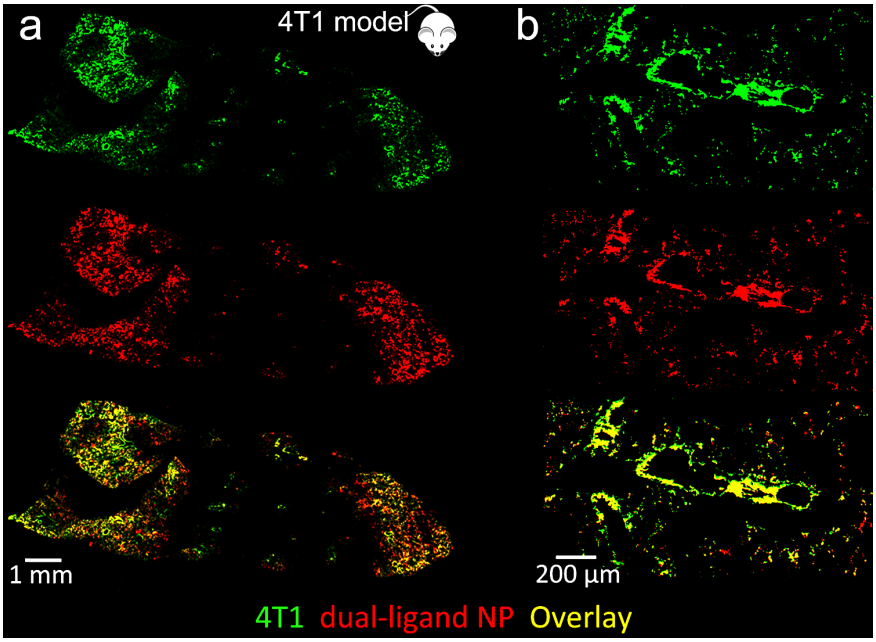

Supporting Figure S5. Histological evaluation of the microdistribution of the dual-ligand nanoparticles in the lungs of mice with 4T1 metastases. (a) Fluorescence image of a histological section of an entire lung lobe (5x magnification). Images of entire histological sections of the lungs were obtained using the automated tiling function of the microscope. The location of dual-ligand NP is shown with respect to metastatic cancer cells in the same histological section (green: 4T1 cancer cells; red: dual-ligand NP; yellow: overlay). **(b)** In higher magnification, the colocalization of dual-ligand NP with metastatic cancer cells is shown (10x).

Supporting Methods: Fabrication of single- and dual-ligand nanoparticles

The DSPE-PEG-ligand was prepared by conjugating the appropriate peptide on DSPE-PEG-NH_2. The same conjugation method was used for the $\alpha_v\beta_3$ integrin-targeting peptide (c(RGDfC), Peptides International) and P-selectin-targeting peptide (CDAEWVDVS, GeneScript). The thiol of the cysteine residue on the peptides was used to conjugate the peptide to the amine of DSPE-PEG-NH_2 *via* the sulfo-SMCC cross-linker for 2 h (Thermo Fisher Scientific). Sulfo-SMCC contains an amine-reactive *N*-hydroxysuccinimide (NHS ester) and a sulfhydryl-reactive maleimide group to form stable amide and thioether bonds. To reassure complete conjugation of the entire amount of DSPE-PEG-NH_2 with the peptide, we used a 2-fold molar excess of the peptides over PEGs. The progression of the reaction was monitored using thin layer chromatography (TLC). TLC was carried out on silica gel coated fiber sheets using a mixture of $CHCl_3$/MeOH as the mobile phase. DSPE-PEG-NH_2 remained at the beginning of the sheets (Rf=0.2), whereas the free peptides migrated to the front of the TLC sheet (Rf =0.78 and 0.85 for PSN and RGD peptide, respectively). In addition to staining with iodine vapor, both spots were ninhydrin positive. The products appeared in a new spot (Rf=~0.55). At the end of the reaction, there were only the spots of DSPE-PEG-peptide and the remaining excess of peptide. The absence of a spot at Rf=0.2 indicated the complete depletion of DSPE-PEG-NH_2. The excess peptide was completely removed using a 1-day dialysis against PBS.

Each nanoparticle variant was labeled with an NIR fluorophore using Vivotag-S 645, Vivotag-S 680, or Vivotag-S 750 (Perkin Elmer), which contained an NHS functional group. The fluorophore was conjugated directly onto the lipid 1,2-Distearoyl-sn-glycero-3-phosphoethanolamine (DSPE) in

chloroform at 55 °C in the presence of triethylamine. To reassure complete conjugation of the entire amount of DSPE with Vivotag, we used a 2-fold molar excess of Vivotag over DSPE. The progression of the reaction was monitored using thin layer chromatography (TLC). At the end of the reaction, there was only the spots of DSPE-Vivotag (Rf= 0.71) and the remaining excess of Vivotag (Rf= 0.86). The absence of a spot at Rf=0.42 indicated the complete depletion of DSPE. The unreacted Vivotag was eventually removed after the liposomes were formed using dialysis. Following evaporation of the solvent, the lipids was used as part of the lipid matrix at 2.5 mol%.

Liposomal nanoparticles were fabricated using established methods.[2] The phospholipids 1,2-dipalmitoyl-sn-glycero-3-phosphocholine (DPPC) and DSPE-PEG(2000)-ligand were used as the lipid matrix for the liposomes. A lipid composition of DPPC, cholesterol and DSPE-PEG(2000)-ligand in the molar ratio of 60-X:40:X was used, where X was 2.5 or 5 mol% for the single-ligand or dual-ligand variants, respectively. The lipids were dissolved in ethanol and hydrated with PBS at 60 °C followed by sequential extrusion in a Lipex Biomembranes Extruder (Northern Lipids, Vancouver, Canada), to size the liposomes to 100 nm. After extrusion, the nanoparticles were dialyzed against PBS for 1 day using a 100 kDa MWCO dialysis tubing (Spectrum Laboratories, CA). The size of the nanoparticles was characterized using dynamic light scattering (DLS, Brookhaven Instruments). The exact number of peptides on each nanoparticle formulation was confirmed using direct protein assays (Bio-Rad Protein Assay using Coomassie Blue G-250 dyes). The final levels of each NIR label on each nanoparticle were directly measured using the FMT system.

Supporting Methods: Phantom studies using Fluorescence Molecular Tomography

Fluorescence Molecular Tomography (FMT) is a technique that shares tomographic principles of diffraction tomography and simultaneously uses absorption and fluorescent measurements for accurate 3-D reconstruction of fluorescent signals. Using NIR fluorescent probes and inversion techniques that take into account the diffuse nature of photon propagation in tissue, previous publications have validated that FMT can accurately measure the absolute concentration of NIR fluorochromes with high positional accuracy in deep tissues.[3,4]

In phantom studies, we investigated the feasibility of simultaneous multichannel measurements of NIR fluorophores. First, we measured the three NIR fluorophores (Vivotag 645, 680 and 750) separately and mixed together using the instrument's phantom sample holder. Using each fluorophore at levels ranging from 100-200 pmoles, the quantification error between FMT measurements of each fluorophore separately or their mixture was less than 5% of the expected concentration for all three fluorochromes. Second, we assessed the quantification accuracy in different depths using commercial chicken breast. We embedded a capillary filled with a mixture of the three fluorochromes (ranging from 5-40 pmoles) in the chicken tissue. We performed measurements at different depths of the tissue to compare near the surface and deep locations. Using the animal holder, multispectral imaging showed a quantification error of 3.8 and 4.9% of the expected concentration for the fluorochromes at a depth of 3 and 18 mm (from the top), respectively.

Supporting Methods: Histological evaluation

Immunohistochemistry was performed on a subset of the animals to evaluate the location of metastatic cancer cells with respect to blood vessels and associated expression of $\alpha_v\beta_3$ integrin and P-selectin. After the last imaging acquisition, the lungs were collected from the mice for histological studies. The animals were anesthetized with an IP injection of ketamine/xylazine and transcardially perfused with heparinized PBS followed by 4% paraformaldehyde in PBS. Organs were explanted and post-fixed overnight in 4% paraformaldehyde in PBS. The tissues were soaked in 30% sucrose (w/v) in PBS at 4 °C for cryosectioning. Serial tissue sections of 12 μm in thickness were stained for the specific endothelial

antigen CD31 and with the nuclear stain DAPI. Direct fluorescence of GFP (green) imaging was performed for imaging the location of metastatic lesions. By conjugating c(RGDfC) and CDAEWVDVS peptides with an Alexa fluorophore, tissue sections were stained for $\alpha_v\beta_3$ integrin and P-selectin. The tissue sections were imaged at 5, 10 or 40x on the Zeiss Axio Observer Z1 motorized FL inverted microscope. To obtain an image of the entire large tissue section (*i.e.*, lung lobe), a montage of each section was made using the automated tiling function of the microscope.

Supporting Methods: Scintigraphic imaging

Instead of an NIR fluorophore, a DTPA chelating agent was conjugated on the surface of the dual-ligand-NP. Briefly, the bifunctional chelator, *p*-SCN-Bn-DTPA agent was conjugated to a fraction of surface amines on the NP in saline solution for 6 h. Each NP contained ~240 DTPA molecules. For ^{99m}Tc radiolabeling, a shake-and-bake method was employed. The nanoparticle suspension contained a 10-fold excess of the chelating agent DTPA over the added ^{99m}Tc radionuclide. Briefly, the reducing agent, $SnCl_2$ (0.3 mg in 0.2 M HCl, purged with nitrogen), was added to 0.5 ml of the dual-ligand-NP suspension (also purged with nitrogen), while the pH of the solution was adjusted close to 7 using a 1M NaOH solution. Sodium pertechnetate (0.3 mCi in saline) was added to the mixture in a shielded vial. The reaction vial was purged with nitrogen, shaken, and stirred for 30 min at 50 °C. Radiochemical purity was confirmed by thin-layer chromatography (radio-TLC). TLC was performed on silica gel coated fiber sheets with 85% aqueous ethanol as the mobile phase. Upon dilution with sterilized PBS to a desired activity of ~20 μCi in an injection volume of 200 μl, each animal was injected with a dose containing ~3×10^{10} nanoparticles.

After tail-vein injection of ~20 μCi of ^{99m}Tc-dual-ligand-NP in 200 μL, whole-body planar gamma scintigraphy images were acquired using a Gamma Medica FLEX small animal-imaging instrument (X-SPECT system) at multiple time points after injection (30 sec acquisition). To verify the findings of the *in vivo* imaging and confirm the presence of metastases in organs, we imaged the lungs *ex vivo* using the Gamma Medica system and a CRi Maestro fluorescence imaging system to detect 4T1 cells expressing GFP (green channel).

References

1. Karathanasis, E.; Chan, L.; Balusu, S. R.; D'Orsi, C. J.; Annapragada, A. V.; Sechopoulos, I.; Bellamkonda, R. V., Multifunctional Nanocarriers for Mammographic Quantification of Tumor Dosing and Prognosis of Breast Cancer Therapy. *Biomaterials* 2008, 29, 4815-4822.
2. Toy, R.; Hayden, E.; Camann, A.; Berman, Z.; Vicente, P.; Tran, E.; Meyers, J.; Pansky, J.; Peiris, P. M.; Wu, H., *et al.*, Multimodal in Vivo Imaging Exposes the Voyage of Nanoparticles in Tumor Microcirculation. *ACS Nano* 2013, 7, 3118-3129.
3. Ntziachristos, V.; Tung, C. H.; Bremer, C.; Weissleder, R., Fluorescence Molecular Tomography Resolves Protease Activity in Vivo. *Nat Med* 2002, 8, 757-760.
4. Montet, X.; Ntziachristos, V.; Grimm, J.; Weissleder, R., Tomographic Fluorescence Mapping of Tumor Targets. *Cancer Res* 2005, 65, 6330-6336.